The Astrophysical Journal, 747:3 (10pp), 2012 March 1 doi:10.1088/0004-637X/747/1/3


# THROUGH THE LOOKING GLASS: BRIGHT, HIGHLY MAGNIFIED GALAXY CANDIDATES AT $z \sim 7$ BEHIND A1703*

L. D. Bradley[1], R. J. Bouwens[2], A. Zitrin[3], R. Smit[2], D. Coe[1], H. C. Ford[4], W. Zheng[4], G. D. Illingworth[5], N. Benítez[6], and T. J. Broadhurst[7,8]
[1] Space Telescope Science Institute, 3700 San Martin Drive, Baltimore, MD 21218, USA
[2] Leiden Observatory, Leiden University, Postbus 9513, 2300 RA Leiden, The Netherlands
[3] School of Physics and Astronomy, Tel Aviv University, Tel Aviv 69978, Israel
[4] Department of Physics and Astronomy, Johns Hopkins University, 3400 North Charles Street, Baltimore, MD 21218, USA
[5] UCO/Lick Observatory, Department of Astronomy and Astrophysics, University of California Santa Cruz, Santa Cruz, CA 95064, USA
[6] Instituto de Astrofísica de Andalucía (CSIC), C/Camino Bajo de Huétor 24, Granada 18008, Spain
[7] Department of Theoretical Physics, University of Basque Country UPV/EHU, Leioa, Spain
[8] Ikerbasque, Basque Foundation for Science, 48011 Bilbao, Spain
*Received 2011 April 11; accepted 2011 December 16; published 2012 February 7*

## ABSTRACT

We report the discovery of seven strongly lensed Lyman-break galaxy (LBG) candidates at $z \sim 7$ detected in *Hubble Space Telescope* Wide Field Camera 3 (WFC3) imaging of A1703. The brightest candidate, called A1703-zD1, has an observed (lensed) magnitude of 24.0 AB ($26\sigma$) in the WFC3/IR F160W band, making it 0.2 mag brighter than the $z_{850}$-dropout candidate recently reported behind the Bullet Cluster and 0.7 mag brighter than the previously brightest known $z \sim 7.6$ galaxy, A1689-zD1. With a cluster magnification of ~9, this source has an intrinsic magnitude of $H_{160} = 26.4$ AB, a strong $z_{850} - J_{125}$ break of 1.7 mag, and a photometric redshift of $z \sim 6.7$. Additionally, we find six other bright LBG candidates with $H_{160}$-band magnitudes of 24.9–26.4, photometric redshifts $z \sim 6.4 - 8.8$, and magnifications $\mu \sim 3$–40. Stellar population fits to the Advanced Camera for Surveys, WFC3/IR, and *Spitzer*/Infrared Array Camera data for A1703-zD1 and A1703-zD4 yield stellar masses $(0.7 - 3.0) \times 10^9\ M_\odot$, stellar ages 5–180 Myr, and star formation rates $\sim 7.8\ M_\odot\ \mathrm{yr}^{-1}$, and low reddening with $A_V \leqslant 0.7$. The source-plane reconstruction of the exceptionally bright candidate A1703-zD1 exhibits an extended structure, spanning ~4 kpc in the $z \sim 6.7$ source plane, and shows three resolved star-forming knots of radius $r \sim 0.4$ kpc.

*Key words:* galaxies: clusters: individual (A1703) – galaxies: high-redshift – gravitational lensing: strong

*Online-only material:* color figures

## 1. INTRODUCTION

The recently installed Wide-Field Camera 3 (WFC3) aboard the *Hubble Space Telescope* (*HST*) has led to a significant increase in the sample of $z \gtrsim 7$ galaxy candidates in the past year (Oesch et al. 2010b; Bouwens et al. 2010a, 2011b; Bunker et al. 2010; McLure et al. 2010; Finkelstein et al. 2010; Trenti et al. 2011; Yan et al. 2011). Already, more than 132 $z \sim 7$–8 Lyman-break galaxy (LBG) candidates (Bouwens et al. 2011b, see also Lorenzoni et al. 2010; McLure et al. 2011) have been found in ultra-deep WFC3/IR observations of the Hubble Ultra-Deep Field (HUDF) and nearby fields, with even a few candidates at $z \sim 8.5$ and one at $z \sim 10$ (Bouwens et al. 2011a). These observations provide our first glimpse of galaxies during the reionization epoch, showing a rapidly evolving galaxy luminosity function (LF) and a declining star formation rate with increasing redshift (Bouwens et al. 2011a, 2011b). Recent studies of these $z \gtrsim 7$ galaxies have also looked at their structure and morphologies (Oesch et al. 2010a), rest-frame $UV$-continuum slopes (Bouwens et al. 2010b; Finkelstein et al. 2010), and star formation rates and stellar masses (Labbé et al. 2010a, 2010b; McLure et al. 2011).

The ultra-deep observations are complemented by shallower wide-field WFC3/IR surveys for $z \gtrsim 7$ galaxies such as the Brightest of Reionizing Galaxies (Trenti et al. 2011) and Hubble Infrared Pure Parallel Imaging Extragalactic Survey (Yan et al. 2011), which so far have uncovered four bright (25.5–26.7) $z \gtrsim 7.5$ galaxies over 130 arcmin$^2$. Over the next three years, the Cluster Lensing And Supernova survey with Hubble (CLASH; Postman et al. 2011) and Cosmic Assembly Near-infrared Deep Extragalactic Legacy Survey (Grogin et al. 2011; Koekemoer et al. 2011) Multi-Cycle Treasury (MCT) programs will further augment the sample of bright $z \gtrsim 7$ galaxy candidates and our understanding of the high-redshift universe. These wide-field surveys are needed to characterize the bright end of the galaxy LF, where bright $z \gtrsim 7$ galaxies are rare. Placing tighter constraints of the number density of bright sources also helps break the degeneracy between the characteristic luminosity $L_*$ and the faint-end slope $\alpha$, a parameter whose value is crucial in determining the contribution of galaxies to the reionization of the universe.

The use of massive galaxy clusters as "cosmic" gravitational telescopes has uncovered some the brightest ($\lesssim$26.5) $z \gtrsim 5$ high-redshift galaxies to date (Franx et al. 1997; Frye et al. 2002; Kneib et al. 2004; Egami et al. 2005; Bradley et al. 2008; Zheng et al. 2009; Bouwens et al. 2009; Hall et al. 2011) and some of the most distant galaxies known at the time of their discovery (Franx et al. 1997; Kneib et al. 2004; Bradley et al. 2008). Gravitational lensing by massive galaxy clusters can amplify both the size and flux of background sources considerably. The increased spatial resolution allows high-redshift galaxies to be

* Based on observations made with the NASA/ESA *Hubble Space Telescope*, obtained at the Space Telescope Science Institute, which is operated by the Association of Universities for Research in Astronomy under NASA contract NAS5-26555. Based on observations made with the *Spitzer Space Telescope*, which is operated by the Jet Propulsion Laboratory, California Institute of Technology under NASA contract 1407.

studied in unprecedented detail, providing clear views of their sizes and morphologies (e.g., Franx et al. 1997; Kneib et al. 2004; Bradley et al. 2008; Zheng et al. 2009; Swinbank et al. 2009). This was clearly demonstrated with a very high source-plane resolution of 50 pc recently achieved by Zitrin et al. (2011) for the $z = 4.92$ galaxy behind MS1358. Likewise, the increased brightness can place $z \gtrsim 7$ galaxies within reach of ground-based spectroscopic follow-up observations.

Luminous high-redshift galaxies are extremely valuable because their spectra can provide direct measurements of the early star formation rate via Ly$\alpha$ and H$\alpha$ emission (Iye et al. 2006) and the evolution of metallicity via metal emission and absorption lines (Dow-Hygelund et al. 2005). The spectra of $z \gtrsim 7$ objects also pinpoint the epoch of the intergalactic medium (IGM) reionization through the effect of neutral hydrogen in inhibiting the emission of Ly$\alpha$ from galaxies (Santos 2004; Malhotra & Rhoads 2004; Stark et al. 2010). A truly neutral IGM will produce a damped Ly$\alpha$ absorption profile (Miralda-Escude & Rees 1998) that can be measured even at a low spectral resolution.

Here we present the discovery of seven bright strongly lensed LBG candidates at $z \sim 7$ behind the massive galaxy cluster A1703. The brightest candidate, A1703-zD1, is observed at 24.0 AB in the $H_{160}$ band, making it 0.2 mag brighter than the $z_{850}$-dropout candidate recently reported behind the Bullet Cluster (Hall et al. 2011) and 0.7 mag brighter than the previously brightest known $z \sim 7.6$ galaxy A1689-zD1, found behind the massive cluster A1689 (Bradley et al. 2008). This paper is organized as follows. We present the observations and photometry in Section 2 and dropout selection in Section 3. In Section 4 we discuss the source magnifications. We present the photometric redshifts in Section 5 and stellar population synthesis models in Section 6. The results and the properties of the sources are discussed in Section 7. We summarize our results in Section 8. Throughout this work, we assume a cosmology with $\Omega_m = 0.3$, $\Omega_\Lambda = 0.7$, and $H_0 = 70$ km s$^{-1}$ Mpc$^{-1}$. This provides an angular scale of 5.2 kpc (proper) arcsec$^{-1}$ at $z = 7.0$. All magnitudes are expressed in the AB photometric system (Oke 1974).

## 2. OBSERVATIONS AND PHOTOMETRY

### 2.1. HST ACS and WFC3/IR Data

We observed A1703 ($z = 0.284$; Allen et al. 1992) with a single field of the Advanced Camera for Surveys (ACS) WFC in 2004 November as part of an ACS GTO program to study five massive galaxy clusters (HST-GO10325). The observations cover a $3\farcm4 \times 3\farcm4$ field of view and consist of 20 orbits divided among six broadband filters: F435W ($B_{435}$; 7050 s), F475W ($g_{475}$; 5564 s), F555W ($V_{555}$; 5564), F625W ($r_{625}$; 9834 s), F775W ($i_{775}$; 11128 s), and F850LP ($z_{850}$; 17800 s). The ACS/WFC data were reduced with our ACS GTO APSIS pipeline (Blakeslee et al. 2003). The reductions reach $5\sigma$ limiting magnitudes ($0\farcs19$ diameter aperture) of 28.5, 28.6, 28.2, 28.6, 28.4, and 28.0 in the $B_{435}$, $g_{475}$, $V_{555}$, $r_{625}$, $i_{775}$, and $z_{850}$ bands, respectively.

We obtained WFC3/IR observations of A1703 in the F125W ($J_{125}$) and F160W ($H_{160}$) bands, each with an exposure time of 2812 s, in 2010 April with the primary goal to search for $z \sim 7$ galaxies (HST-GO11802). The WFC3/IR observations cover the central $123'' \times 136''$ high-magnification region of the cluster (see Figure 1). The depths of the WFC3/IR data reach $5\sigma$ limiting magnitudes of 27.3 and 26.9 in a $0\farcs45$ diameter aperture for the $J_{125}$ and $H_{160}$ bands, respectively.

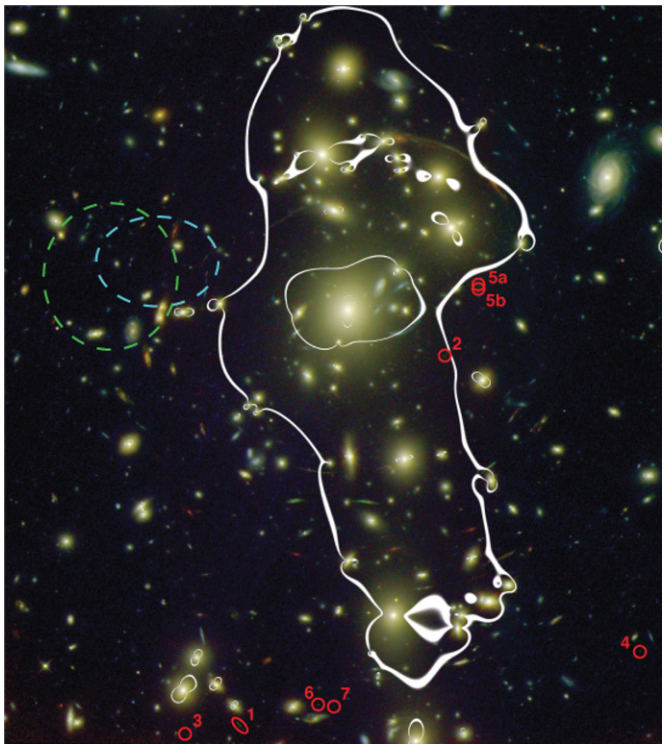


**Figure 1.** Color image ($z_{850}J_{125}H_{160}$) of the galaxy cluster A1703 ($z = 0.28$). The locations of the high-redshift $z_{850}$-dropout candidate galaxies are marked by red circles and ellipses. The image field of view is $123'' \times 136''$ and is shown with a position angle = 152°. The white contours represent the critical curves at $z \sim 7$. The dashed cyan and green ellipses denote the regions where the strong lensing model of Zitrin et al. (2010) predicts counterimages for A1703-zD2 and A1703-zD5a/5b, respectively.

(A color version of this figure is available in the online journal.)

For the reduction of both the ACS and WFC3/IR data, we weight each individual exposure by its inverse variance created from the sky background, modulated by the flat-field variations, along with the read noise and dark current. The drizzle combination procedure uses these inverse-variance images as weights and produces a final inverse-variance image for the combined, drizzled image in each filter. These inverse-variance weight images are used by SExtractor (Bertin & Arnouts 1996) for both source detection and photometry (see Section 2.3).

### 2.2. Spitzer/IRAC Data

We utilized archival *Spitzer*/Infrared Array Camera (IRAC) imaging of A1703 (program 40311) obtained over three epochs between 2007 December and 2008 June. We used the *Spitzer* MOPEX calibration pipeline to combine the data in the 3.6 and 4.5 $\mu$m bands over the three epochs. The total exposure times were 18.9 ks in the 3.6 and 4.5 $\mu$m bands, reaching $5\sigma$ limiting magnitudes of 24.7 and 24.1, respectively.

### 2.3. Photometry

We used SExtractor in dual-image mode for object detection and photometry. The detection image consisted of an inverse-variance weighted combination of the WFC3/IR $J_{125}$ and $H_{160}$ images. We smoothed the ACS optical images to match the WFC3/IR images and measured colors in small scalable Kron apertures (Kron factor of 1.2; Kron 1980). We then correct the fluxes measured in these smaller apertures to total magnitudes by using the flux measured in a larger Kron aperture (factor

**Table 1**
Observed Photometry of High-redshift Candidates

| Candidate | R.A. | Decl. | $z_{850}$ | $J_{125}$ | $H_{160}$ | 3.6 $\mu$m | 4.5 $\mu$m | $\mu$[a] | $z_{\rm phot}$[b] |
|---|---|---|---|---|---|---|---|---|---|
| A1703-zD1 | 13:14:59.4183 | 51:50:00.843 | $25.8 \pm 0.20$ | $24.1 \pm 0.04$ | $24.0 \pm 0.06$ | $23.9 \pm 0.1$ | $24.7 \pm 0.4$ | $9.0^{+0.9}_{-4.4}$ | $6.7^{+0.2}_{-0.1}$ |
| A1703-zD2 | 13:15:06.5089 | 51:49:17.960 | $25.6 \pm 0.20$ | $24.9 \pm 0.10$ | $24.9 \pm 0.14$ | ... | ... | $24.8^{+43.6}_{-10.4}$ | $6.4^{+0.1}_{-0.3}$ |
| A1703-zD3 | 13:14:58.3860 | 51:49:57.740 | $26.8 \pm 0.48$ | $25.5 \pm 0.14$ | $25.1 \pm 0.15$ | ... | ... | $7.3^{+1.3}_{-2.5}$ | $6.7^{+1.6}_{-0.2}$ |
| A1703-zD4 | 13:15:07.1889 | 51:50:23.552 | $> 28.0$ | $25.5 \pm 0.10$ | $25.4 \pm 0.13$ | $25.6 \pm 0.5$ | $24.7 \pm 0.5$ | $3.1^{+0.2}_{-1.0}$ | $8.4^{+0.9}_{-1.4}$ |
| A1703-zD5a[c,d] | 13:15:07.7650 | 51:49:09.333 | $26.7 \pm 0.34$ | $25.6 \pm 0.12$ | $25.7 \pm 0.18$ | ... | ... | $39.0^{+26.9}_{-15.0}$ | $6.5^{+0.2}_{-0.3}$ |
| A1703-zD5b[c] | 13:15:07.7036 | 51:49:10.139 | $26.3 \pm 0.29$ | $25.3 \pm 0.11$ | $25.3 \pm 0.15$ | ... | ... | $26.9^{+19.9}_{-8.0}$ | $6.5^{+0.2}_{-0.2}$ |
| A1703-zD6[e] | 13:15:01.0068 | 51:50:04.353 | $27.9 \pm 0.53$ | $25.8 \pm 0.08$ | $25.9 \pm 0.12$ | ... | ... | $5.2^{+0.3}_{-0.9}$ | $7.0^{+0.6}_{-0.2}$ |
| A1703-zD7 | 13:15:01.2696 | 51:50:06.052 | $>28.5$ | $26.8 \pm 0.22$ | $26.4 \pm 0.21$ | ... | ... | $5.1^{+0.4}_{-0.9}$ | $8.8^{+0.2}_{-1.7}$ |

**Notes.** The sources without quoted IRAC magnitudes either suffer from significant confusion from neighboring sources or do not show an especially prominent ($>2\sigma$) detection.

[a] The magnification errors represent the extreme values obtained from the minimum and maximum magnifications obtained within $\pm 0\farcs5$ of each candidate and assuming $\Delta z \pm 1.0$ for the source redshifts.

[b] Photometric redshifts determined from the BPZ code (Benítez 2000). Because of the limited depth of the optical data, there is a small chance that some of the sources could be at low redshift (see Section 5).

[c] As discussed in the text, A1703-zD5a and A1703-zD5b most likely represent two star-forming knots within a single source. The magnification of the combined A1703-zD5 source is $31.9^{+20.3}_{-10.6}$.

[d] This component of the zD5 candidate is detected in the $V_{555}$ band at low significance ($2.1\sigma$), but not in the overlapping $g_{475}$ and $r_{625}$ bands. Thus, the slight $V_{555}$-band detection is likely a statistical fluctuation.

[e] This candidate is spectroscopically confirmed to be at $z = 7.045$ (Schenker et al. 2012).

of 2.5) on the detection image. Likewise, we apply aperture corrections for light falling outside of the large Kron aperture using the tabulated encircled energies provided in the instrument handbooks.

We were able to obtain *Spitzer*/IRAC fluxes for only two of the brighter and isolated sources. IRAC fluxes for these candidates were obtained using the deblending algorithm of Labbé et al. (2006, 2010b). Briefly, this method involved using the higher resolution *HST* WFC3/IR images to create model IRAC images for the source and its nearby neighbors (assuming no differences between the structure or size of sources at 1.25 microns and IRAC wavelengths). We then vary the normalization of each model image, for both the source and its nearby neighbors, to fit the IRAC observations. Finally, we subtract the best-fit model profiles for the neighbors and perform photometry for the sources of interest in a $2\farcs5$-diameter aperture. The IRAC errors include a component due to the modeling error. The modeling error can be quite large for sources near the edges of the WFC3/IR image because there is no source template for IRAC sources found beyond the WFC3/IR field of view.

## 3. SELECTION OF $z \sim 7$ $z_{850}$-BAND DROPOUT CANDIDATES

We search for $z \sim 7$ galaxies using a $z_{850}$-dropout selection criterion in two colours, based on the magnitudes measured in the small scalable apertures. We require candidates to have $z_{850} - J_{125} \geqslant 0.7$ and $J_{125} - H_{160} < 0.5$. In addition, they must be undetected ($<2\sigma$) in each optical ACS band, with not more than one band showing a $>1.5\sigma$ detection. Further, candidates must be detected at $>5\sigma$ in the $J_{125}$ band. In cases where an object is not detected in a particular band, we assign the object with the $1\sigma$ detection limit to calculate object colors.

Because our $z_{850} - J_{125}$ color criterion is slightly bluer than the $z_{850} - J_{125} > 0.9$ used by Bouwens et al. (2011b), we effectively extend our redshift selection window to somewhat lower redshifts. The use of the Bouwens et al. (2011b) color criterion, which was explicitly chosen to exclude source with redshifts $z < 6.5$, would eliminate only one of our candidates.

Using these colour criteria, we identified seven $z_{850}$-dropout galaxy candidates with observed $H_{160}$-band magnitudes between 24.0 and 26.4. The candidates are named in decreasing order of their brightness in the $H_{160}$ band, with the exception of the close pair of A1703-zD5a and A1703-zD5b. As discussed in the next section, A1703-zD5a and A1703-zD5b most likely represent two star-forming knots within a single source. We note that the A1703-zD5a component is detected in the $V_{555}$ band at low significance ($2.1\sigma$), but not in the overlapping $g_{475}$ and $r_{625}$ bands. Thus, we interpret the slight $V_{555}$-band detection as a likely statistical fluctuation.

All of the candidates are clearly resolved with the exceptions of our two faintest two candidates, A1703-zD6 and A1703-zD7. A1703-zD6 is unresolved with SExtractor stellarity parameter of 0.97. A1703-zD7 is somewhat extended, but only slightly resolved with a stellarity parameter of 0.5. Because A1703-zD6 is unresolved, under normal circumstances it cannot be ruled out as a low-mass L,T dwarf star. However, this candidate has subsequently been confirmed to be at $z = 7.045$ with deep Keck spectroscopic observations (Schenker et al. 2012).

While the WFC3/IR data were taken after the ACS optical data, we can rule we rule out supernovae as contaminants to our sample because the sources are either resolved or in the case of the unresolved source A1703-zD6, spectroscopically confirmed at $z = 7.045$.

The positions of these sources in the A1703 data are shown in Figure 1. Their properties are listed in Table 1 and cutout stamps showing each of the sources are presented in Figure 2. The $z_{850} - J_{125}$ and $J_{125} - H_{160}$ colors of the candidates are illustrated in Figure 3. As seen in this figure, the $z_{850} - J_{125}$ color of A1703-zD2 is exactly at our selection limit (0.7). While it could be in our $z \sim 7 z_{850}$-dropout sample as a result of photometric scatter, this candidate is completely undetected in the deep optical ACS data. Its somewhat bluer $z_{850} - J_{125}$ color means it is at the lower-redshift edge of our $z_{850}$-dropout selection window. This is completely consistent with its photometric

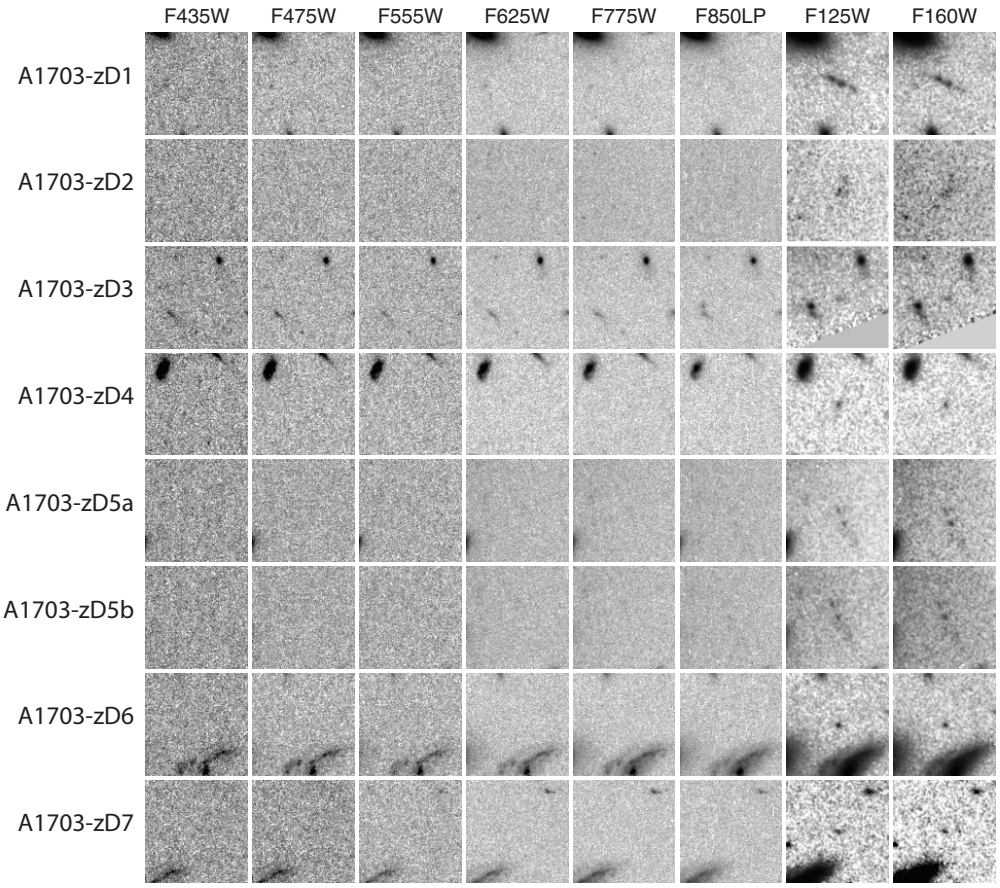


**Figure 2.** Postage stamp cutout images of the high-redshift $z_{850}$-dropout candidate galaxies from the *HST* ACS and WFC3/IR data. The cutout images are $6'' \times 6''$, corresponding to 31.4 kpc on a side at $z = 7$, and are shown with a position angle = 130°. As discussed in the text, A1703-zD5a and A1703-zD5b most likely represent two star-forming knots within a single source.

redshift of $z = 6.4$ (see Section 5), making it our lowest redshift candidate.

The best candidate, A1703-zD1, is an extremely bright $z_{850}$-dropout candidate, with a $H_{160}$ magnitude of 24.0, that appears to be resolved in three separate knots (see Figure 2 and Section 7.2). In Figure 4 we present a histogram of both the observed and intrinsic (unlensed) $H_{160}$ magnitudes compared with the 73 $z \sim 7$ candidates found in the HUDF09 and its two parallel fields and the WFC3/IR Early Release Science observations (Bouwens et al. 2011b).

## 4. SOURCE MAGNIFICATIONS AND COUNTERIMAGES

Several detailed studies to model the lensing of A1703 have been performed in recent years (Limousin et al. 2008; Richard et al. 2009; Zitrin et al. 2010). We adopt the Zitrin et al. (2010) A1703 strong lensing model to estimate the magnifications of the seven $z \sim 7$ sources and to identify possible counterimages. Zitrin et al. (2010) used 16 multiply imaged systems behind A1703 and applied two independent strong lensing techniques to the high-quality, multiband ACS data, yielding similar results. Their strong lensing model places tight constraints on the inner mass profile, and thus provides reliable magnification estimates for background sources. The magnifications of the high-redshift candidates range from $\mu \sim 3$ to large magnifications of ~25–40, found for three of our sources that are located near the critical curve, where the magnification formally diverges. The magnification of each candidate is presented in Table 1.

We estimated the magnification uncertainties by taking models extracted from the $1\sigma$ confidence level, as determined by the $\chi^2$ minimization of model, and marginalizing over the true $1\sigma$ errors. To make the error estimates more conservative, we also incorporate the range of magnifications obtained within $\pm 0\farcs5$ of each candidate and apply a $\Delta z \pm 1.0$ to the redshift of each source. Thus, the $\pm 0\farcs5$ shift is a measure of the magnification variance around the location of the source and the application of $\Delta z \pm 1.0$ accounts for the possible local uncertainty in the location of the critical curves. For objects that are close to the critical lines, the magnification errors are diverging due to their proximity to the critical curve, while objects far away will have a well-determined magnification as the latter slowly varies in regions away from the critical curve.

The brightest candidate, A1703-zD1, has a magnification of ~9, giving it an intrinsic magnitude of ~26.4 in the $H_{160}$ band. The A1703 strong lensing model predicts counterimages for the three high-magnification candidates, A1703-zD2 and the pair of A1703-zD5a and A1703-zD5b, which are located nearby or on the high-redshift critical curve (see Figure 1). The lensing model predicts three counterimages for A1703-zD2 ($\mu = 24.8$; see Figure 1). Taking into account the much smaller magnifications ($\mu = 5.5$–$9.0$) of the counterimages, they are predicted to have $H_{160}$ magnitudes between 26.0 and 26.5. This is sufficiently bright that there was some possibility that we might locate them, but also a good chance we might not because they could easily be lost in the wings of a foreground galaxy. Despite an extensive search, we did not find any viable $z \sim 7$ candidates near the predicted positions of the counterimages.

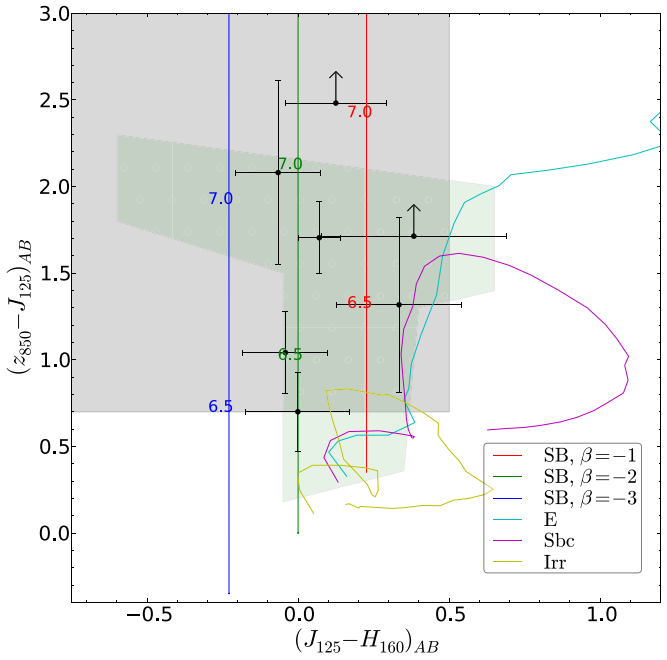


**Figure 3.** $z_{850} - J_{125}$ vs. $J_{125} - H_{160}$ two-color diagram used to select the $z_{850}$-band dropout candidates. The error bars and lower limits are $1\sigma$. The gray region represents the $z_{850} - J_{125}$ and $J_{125} - H_{160}$ colors of the selection criteria. The blue, green, and red lines show the expected colors of star-forming galaxies with UV-continuum slopes of $\beta = -1$, $-2$, and $-3$ ($f_\lambda \propto \lambda^\beta$), respectively. The cyan, magenta, and yellow lines depict the expected colors of low-redshift interloper galaxies. The green region indicates the colors of low-mass L,T dwarf stars (e.g., Knapp et al. 2004). While there is considerable overlap in the colors of L,T stars, only one of the $z_{850}$-dropout candidates (A1703-zD6) is unresolved. However, this candidate has been subsequently spectroscopically confirmed at $z = 7.045$ (Schenker et al. 2012).

(A color version of this figure is available in the online journal.)

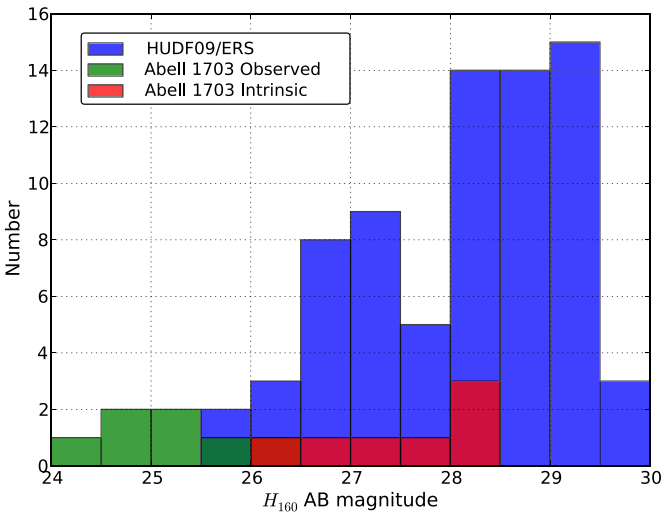


**Figure 4.** Histogram of the observed and intrinsic (unlensed) $H_{160}$ magnitudes for the seven $z_{850}$-dropout ($z \sim 7$) candidate galaxies identified behind A1703 (green and red) compared with the 73 $z \sim 7$ candidates found in the HUDF09 and its two parallel fields and the WFC3/IR Early Release Science observations (blue; Bouwens et al. 2011b).

(A color version of this figure is available in the online journal.)

The close pair of A1703-zD5a and A1703-zD5b are also located in very close proximity of the critical curve and as such have high magnifications of $\mu \sim 27$–$40$. These candidates are also predicted to have counterimages on the other side of the brightest cluster galaxy (see Figure 1) with magnifications of $\mu = 5.5$, about five times less than A1703-zD5b. The predicted counterimages are expected to have an $H_{160}$ magnitude of $\geqslant$27.0, which is fainter than our $5\sigma$ limiting magnitude of 26.9. Hence, it is not surprising that no $z_{850}$-dropout candidates are found in the predicted region of the counterimages.

The critical curve lies only 2.″6 from passing between the A1703-zD5a and A1703-zD5b sources, which is within the model (and redshift) uncertainty. To test the hypothesis that these two candidates are multiple images of the same source, we constructed a new model assuming that zD5a and zD5b are the same object. The resulting model is physically plausible and the predicted counterimage of this system, located in the same region marked in Figure 1, is again fainter than the $5\sigma$ limiting magnitude of 26.9. Because the overall reproduction of all other systems remains the same, we cannot exclude this option based solely on the mass model. This possibility could also be supported by their similar colors, morphologies, and photometric redshifts.

However, because surface brightness is conserved in lensing, zD5a and zD5b should have the same surface brightness if they are indeed the same source. For zD5a and zD5b, we find surface brightnesses of 25.9 and 25.8 mag arcsec$^{-2}$, respectively, in the $J_{125}$ band and 26.4 and 25.9 mag arcsec$^{-2}$, respectively, in the $H_{160}$ band. We note that these results are consistent with Oesch et al. (2010a) who found a mean $J_{125}$band observed surface brightness of $\sim$26 mag arcsec$^{-2}$ for a sample of $z \sim 7$ $z_{850}$-band dropouts candidates spanning 26 to 29 mag in the $J_{125}$ band. While their surface brightness agrees in the $J_{125}$ band, zD5b has a brighter surface brightness in the $H_{160}$ band. On these grounds we conclude that zD5a and zD5b are two unique sources. Further, their very close proximity of 0.″76 in the image plane, with a magnification of 8.6 along the line separating them, translates to only $\sim$480 pc in the source plane. Thus, even though we do not observe a diffuse component, which could have very low surface brightness below our detection limits, between them, we conclude that zD5a and zD5b are most likely two star-forming knots within a single source. The magnification of the combined A1703-zD5 source is $31.9^{+20.3}_{-10.6}$. We refer to the these sources separately because they appear as distinct sources in our catalog. The small elliptical Kron apertures used to measure their colors are well separated with sizes of 0.″34 × 0.″26 and 0.″28 × 0.″22, respectively.

We also considered the possibility that zD5a/b and zD2 were all counterimages of the same source. With zD5a/b representing two bright star-forming knots in a single candidate galaxy and not counterimages of the same source, we conclude that zD2 cannot be a counterimage of the zD5a/b source based simply on morphology. This was verified by constructing an additional model considering the center of zD2 and the center of zD5a/b as counter positions of the same source.

## 5. PHOTOMETRIC REDSHIFTS

To estimate the redshifts of the candidates, we used the Bayesian photometric redshift (BPZ) code (Benítez 2000; Benítez et al. 2004; Coe et al. 2006). Briefly, the photometric redshifts are based on a $\chi^2$-fitting procedure to template spectra. Because the shape of the redshift distribution is not well calibrated at $z \sim 7$, we assumed a flat prior for all redshifts. The photometric redshifts of the $z_{850}$-dropout candidates are presented in Table 1 and their posterior $P(z)$ probability distributions are shown in Figure 5. We find redshifts in the range of $z_{\rm phot} = 6.4$–$8.8$, with a median redshift of 6.7.

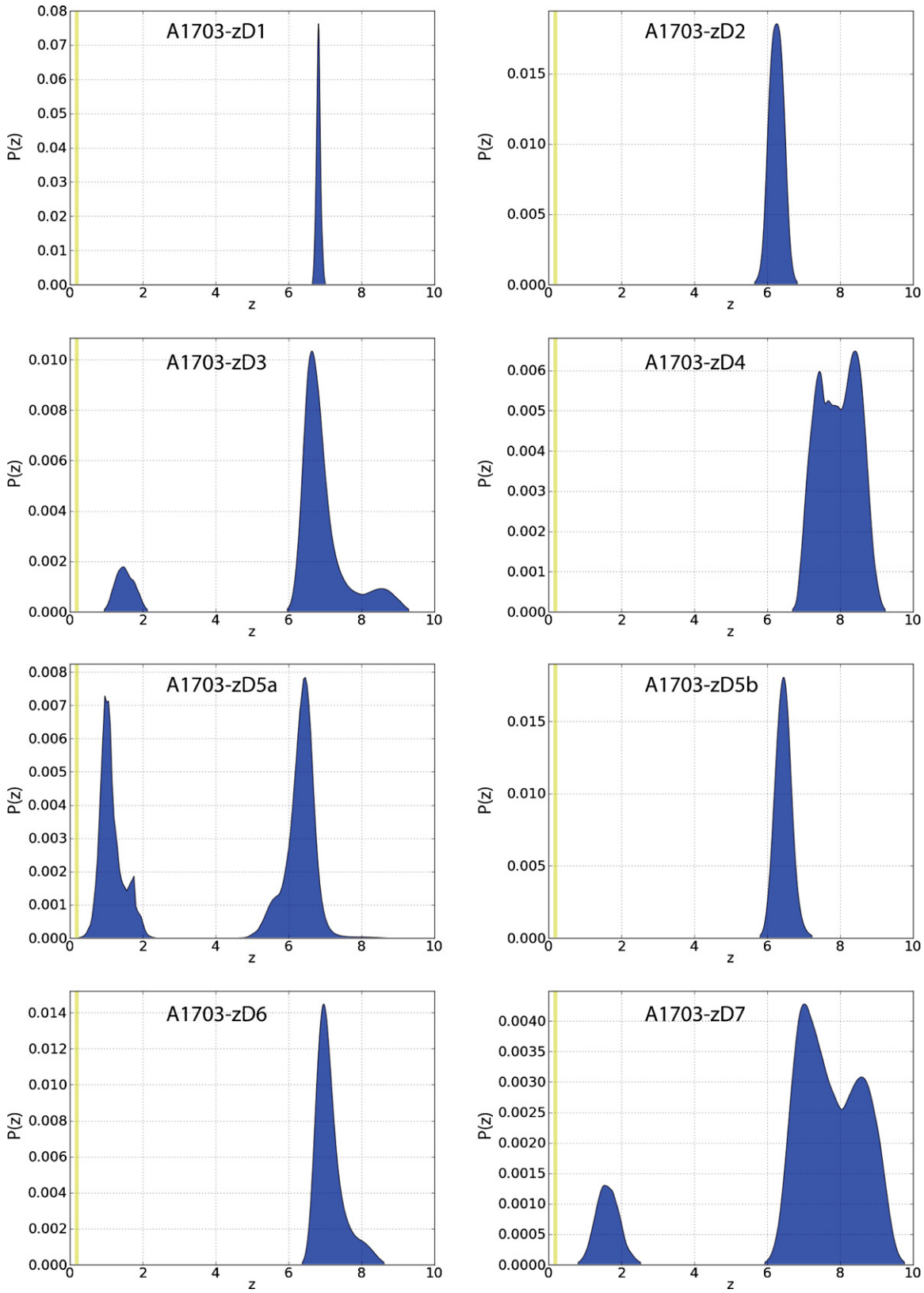


**Figure 5.** Probability distributions of the photometric redshifts for each of the candidates. The vertical yellow line represents the redshift of the A1703 cluster ($z = 0.28$). As discussed in the text, A1703-zD5a and A1703-zD5b most likely represent two star-forming knots within a single source. The A1703-zD5a component shows the highest probability of being at low redshift due to its modest $2.1\sigma$ detection in the F555W band, which we attribute to a statistical fluctuation as described in the text.

(A color version of this figure is available in the online journal.)

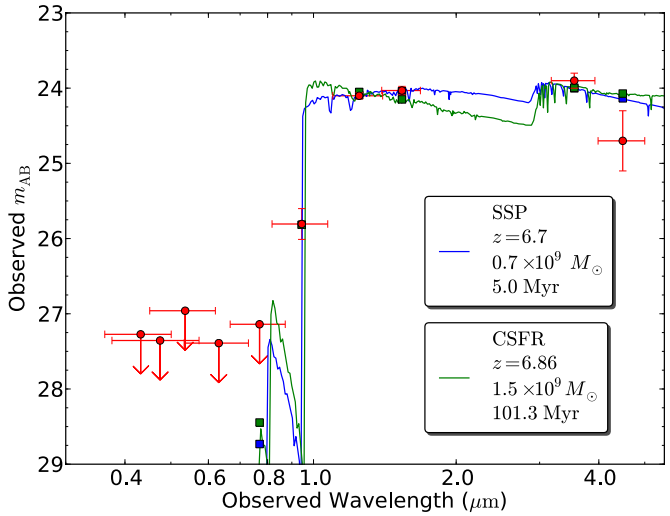


**Figure 6.** Best-fit stellar population models to the observed multiband photometry of A1703-zD1. The models assume a Salpeter (1955) IMF with subsolar ($Z = 0.2\,Z_\odot$) metallicity. The $2\sigma$ upper limits are shown for the ACS optical non-detections, but the models were fit to the measured fluxes and errors. The stellar masses are intrinsic values, corrected for the cluster magnification. The larger $\chi^2_\nu$ values (1.3–2.4) for these models results from the poor fit to the IRAC 4.5 $\mu$m-band data.

(A color version of this figure is available in the online journal.)

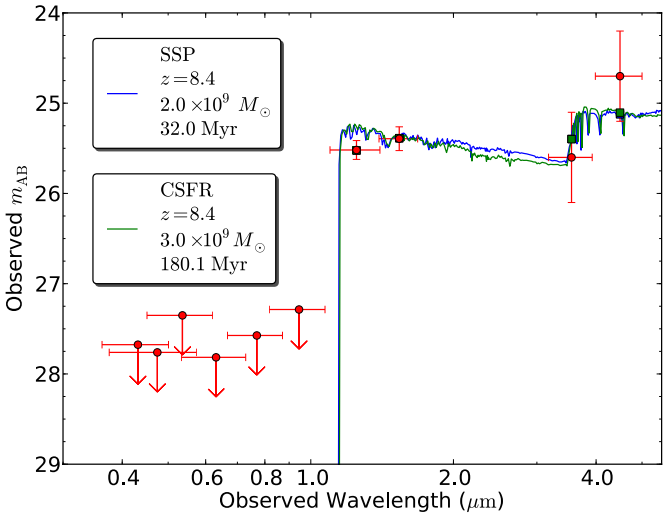


**Figure 7.** Best-fit stellar population models to the observed multiband photometry of A1703-zD4. The models assume a Salpeter (1955) IMF with subsolar ($Z = 0.2\,Z_\odot$) metallicity. The $2\sigma$ upper limits are shown for the ACS optical non-detections, but the models were fit to the measured fluxes and errors. The stellar masses are intrinsic values, corrected for the cluster magnification.

(A color version of this figure is available in the online journal.)

The posterior probability distributions show that there is a small chance that A1703-zD3, A1703-zD5a, and A1703-zD7 could be at low redshift. Because of the modest $2.1\sigma$ detection in the F555W band, the A1703-zD5a knot shows the highest probability of being at low redshift. While we cannot completely exclude the low-redshift solutions for these candidates, objects in this magnitude range (24.0–26.4) with colors similar to LBGs would be rare and are more likely to be at high redshift. The BPZ results indicate that the exceptionally bright candidate A1703-zD1 has a narrow probability distribution at $z = 6.7$ and has the highest probability of being at high redshift, not showing any evidence to suggest a low-redshift solution.

## 6. STELLAR POPULATION MODELS

We performed fits to the multiband *HST* and *Spitzer* photometry of A1703-zD1 and A1703-zD4 using the stellar population models of Bruzual & Charlot (2003). We adopted a Salpeter (1955) initial mass function (IMF) with mass cutoffs of 0.1 and 100 $M_\odot$ and models with subsolar ($Z = 0.2\,Z_\odot = 0.004$) metallicities. The effect of dust reddening is included in the models using the Calzetti et al. (2000) obscuration law. We use the Madau (1995) procedure to correct the models for Lyman-series line-blanketing and photoelectric absorption. The stellar population models are constrained such that the stellar age must be less than the age of the universe at the fit redshift (e.g., 0.75 Gyr at $z = 7.0$). We consider two star formation histories (SFHs): simple (single-burst) stellar population (SSP) models and constant star formation rate (CSFR) models.

The best-fit stellar population models for A1703-zD1 and A1703-zD4, the two sources for which we were able to obtain IRAC photometry, are shown in Figures 6 and 7, respectively and the parameters are given in Table 2. For these sources we find reasonably good model fits to the observed broadband photometry. For A1703-zD1, we note that the spectral energy distribution (SED) models are unable to fit the low flux in the IRAC 4.5$\mu$m band, resulting in a somewhat higher $\chi^2_\nu = 1.3$–2.4

We find intrinsic (unlensed) stellar masses for both candidates in the range (0.7–3.0) $\times$ 10$^9$ $M_\odot$ with star formation rates of 7.3 $\pm$ 0.3 $M_\odot$ yr$^{-1}$and 8.2 $\pm$ 1.2 $M_\odot$ yr$^{-1}$, broadly consistent with those found for $z \sim$ 6–8 galaxy candidates (Labbé et al. 2010a, 2010b; Gonzalez et al. 2011; McLure et al. 2011). Because these two candidates are located near the edge of the WFC3/IR field, there are no source templates for IRAC sources found beyond the WFC3/IR field of view. This results in a large modeling error for the neighboring sources, which we include in the total IRAC error for these candidates. While our modeling procedure weights each photometric data point by its inverse variance, because of the relatively large IRAC errors for these sources it should be noted that there is a larger uncertainty in the resulting stellar masses and ages derived from the stellar population models.

While we assumed a Salpeter IMF, fitting models using a Chabrier (2003) IMF would yield lower masses and star formation rates by a factor $\sim$1.5. For both candidates, we note that the CSFR models provide consistently older SFR-weighted mean stellar ages than those for the SSP models. We find CSFR models with weighted ages of 100–180 Myr, values again similar to that recently reported for a sample of $z \sim$ 7–8 candidates (Labbé et al. 2010b; McLure et al. 2011).

## 7. DISCUSSION

### 7.1. A1703-zD1 Brightness

Some of the brightest ($\lesssim$ 26.5) $z \gtrsim 5$ high-redshift galaxies to date (Franx et al. 1997; Frye et al. 2002; Kneib et al. 2004; Egami et al. 2005; Bradley et al. 2008; Zheng et al. 2009; Bouwens et al. 2009; Hall et al. 2011) have been identified in searches behind strong lensing clusters. Several of the more notable examples include the bright $i_{775}$-dropout galaxy, A1703-iD1, found by Zheng et al. (2009) behind A1703. This candidate has a NICMOS/NIC3 $H_{160}$-band magnitude of 23.9 and is lensed by a factor $\mu \sim 3.1$. From the SED fitting of this source, we found a photometric redshift of $z = 5.95 \pm 0.15$, which is consistent with the Keck spectroscopic redshift of $z = 5.827$ measured by Richard et al. (2009).

**Table 2**
Best-fit Stellar Population Model Results

| Candidate | SFH[a] | $z_{\rm phot}$[b] | Mass[c] ($10^9\ M_\odot$) | Age$_w$[d] (Myr) | SFR ($M_\odot\ {\rm yr}^{-1}$) | $A_V$ | $\chi^2_\nu$ |
|---|---|---|---|---|---|---|---|
| A1703-zD1 | SSP | $6.7 \pm 0.1$ | $0.7 \pm 0.1$ | 5.0 | ... | $0.7 \pm 0.1$ | 1.3 |
| | CSFR | $6.86 \pm 0.1$ | $1.5 \pm 0.05$ | 101.3 | $7.3 \pm 0.3$ | $0.00 \pm 0.00$ | 2.4 |
| A1703-zD4 | SSP | $8.4 \pm 0.3$ | $2.0 \pm 1.4$ | 32.0 | ... | $0.09^{+0.29}_{-0.09}$ | 0.8 |
| | CSFR | $8.4 \pm 0.3$ | $3.0 \pm 0.4$ | 180.1 | $8.2 \pm 1.2$ | $0.0 \pm 0.0$ | 0.8 |

**Notes.** Models assume a Salpeter (1955) IMF with mass cutoffs of 0.1 and 100 $M_\odot$ and subsolar ($Z = 0.2\ Z_\odot = 0.004$) metallicities.
[a] Star formation history: simple (single-burst) stellar population (SSP) or constant star formation rate (CSFR) models.
[b] Photometric redshifts derived from the stellar population fitting. These redshifts are consistent with those presented in Table 1.
[c] Best-fit stellar mass, corrected by the magnification at the fitted $z_{\rm phot}$ redshift.
[d] SFR-weighted mean stellar age (cf. Förster Schreiber et al. 2004). For a CSFR model, the weighted age is simply half of the time elapsed since the start of star formation.

At somewhat higher redshift, Kneib et al. (2004) identified an exceptionally bright candidate (NIC3 $H_{160}$= 24.1) behind the galaxy cluster A2218. This triply imaged candidate, A2218-iD1, lies near the high-redshift critical curve and has a large magnification of $\mu \sim 25$. While this very bright candidate has a similar $H_{160}$-band magnitude as A1703-zD1 and has been suggested to be at $z \sim 7$, it has a $z_{850} - J_{110}$ color of just ∼0.4 mag, which is more consistent with a redshift of $z = 6.3 \pm 0.1$. It therefore almost certainly has a lower redshift than the present candidate A1703-zD1 and A1689-zD1, which is the brightest $z \sim 7.6$ candidate known. A1689-zD1 was discovered by Bradley et al. (2008) behind the massive galaxy cluster A1689. This source is magnified by a factor of $\mu \sim 9.3$ and has a NIC3 $H_{160}$ magnitude of 24.7, which is 0.7 mag fainter than the exceptionally bright candidate $z \sim 7$ candidate A1703-zD1 presented here. Most recently, Hall et al. (2011) reported the discovery of a very bright $z_{850}$-dropout candidate behind the Bullet Cluster. The lensing model of the Bullet Cluster suggests that this candidate is doubly imaged with observed $H_{160}$-band magnitudes of 24.2 and 25.0 and magnifications of 8.4 and 12, respectively. However, because this candidate is detected in the $i_{775}$ band, there is a fair chance this object could be a low-redshift interloper (Hall et al. 2011).

### 7.2. A1703-zD1 Source-plane Reconstruction and Morphology

The large magnification of A1703-zD1 allows us an opportunity to examine the morphology of this exceptionally bright $z \sim 6.7$ galaxy candidate at very high spatial resolution. With a magnification of $\mu \sim 9$, the strong lensing effect provides an increased spatial resolution by about a factor ∼3 compared to an unlensed source. This permits us to resolve spatial structures that would otherwise be unobservable in high-redshift $z \sim 7$ galaxies.

We used the Zitrin et al. (2010) A1703 cluster lensing model to reconstruct A1703-zD1 in the source plane at $z \sim 6.7$. The deprojected image of A1703-zD1 in the WFC3/IR $J_{125}$ band is shown in Figure 8. The linear magnification along the shear direction is $4.88^{+0.11}_{-0.14}$ and $1.84 \pm 0.01$ in the direction perpendicular to the shear direction. This candidate appears to be comprised of three resolved star-forming knots, each with a radius $r \sim 0\farcs08$ (0.4 kpc) in the source plane. Altogether, A1703-zD1 has an extended linear morphology that spans $\sim 0\farcs74$ (∼4 kpc) in the source plane at $z = 6.7$. Of course the physical size and structure we infer for this candidate is somewhat dependent on the details of the gravitational lensing model.

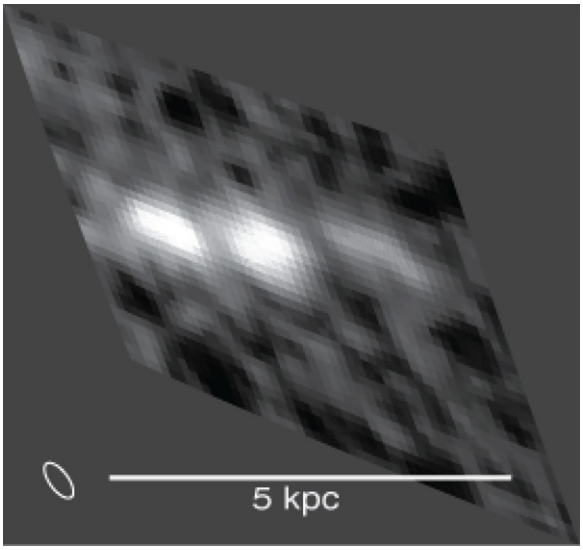


**Figure 8.** Source-plane reconstruction of A1703-zD1 in the WFC3/IR $J_{125}$ band. The source has an extended morphology that spans $\sim 0\farcs74$ (∼4 kpc) in the source plane at $z = 6.7$. A1703-zD1 is comprised of three separate resolved knots, each with radius $r \sim 0\farcs08$ (∼0.4 kpc). Of course the physical size and structure we infer for this candidate is somewhat dependent on the details of the gravitational lensing model. The white ellipse denotes the WFC3/IR $J_{125}$ point-spread function in the source plane ($0\farcs16$ FWHM in the image plane).

There are now several examples of $z \gtrsim 5$ lensed galaxy candidates that have morphologies consisting of star-forming knots (Franx et al. 1997; Kneib et al. 2004; Bradley et al. 2008; Zheng et al. 2009; Swinbank et al. 2009; Zitrin et al. 2011). Interestingly, each of the bright lensed candidates discussed in the previous section are extended and show significant substructure. In particular, both A1703-iD1 and A1689-zD1 show a pair of resolved star-forming knots. Additionally the pair of $z \sim 6.5$ dropout candidates, CL0024-iD1 and CL0024-zD1, each seem to consist of two components. With a separation of only 2 kpc in the source plane and nearly identical redshifts and properties (Zheng et al. 2009), it is possible that CL0024-iD1 and CL0024-zD1 are spatially associated or merging galaxies. Recently, Oesch et al. (2010a) even found extended features with resolved double cores in two unlensed $z \sim 7$ galaxies identified in the WFC3/IR HUDF. The apparent frequency of high-

redshift galaxies showing substructure and multiple components is perhaps not surprising, but it provides strong evidence that both clumpy star formation and merging are important aspects of galaxy buildup at these very early epochs in the universe. The existence of substantial substructure is also expected based on studies of low-redshift Lyman-break analog galaxies (Overzier et al. 2008).

### 7.3. Number Counts of $z \sim 7$ Candidates

The discovery of seven $z \sim 7$ $z_{850}$-dropout candidates in a single cluster field is quite remarkable, especially since four of our candidates (zD1, zD3, zD6, and zD7) lie in a small region near the edge of the WFC3/IR image. While this may be surprising and call into question the reliability of these candidates, our confidence is bolstered by the spectroscopic confirmation at $z = 7.045$ (Schenker et al. 2012) of A1703-zD6, the second-faintest candidate. We consider the extremely bright ($H_{160} = 24.0$) candidate A1703-zD1, with a strong $z_{850} - J_{125}$ break of 1.7, to be a rather robust high-redshift candidate, but we acknowledge that A1703-zD7, the faintest and nearly unresolved candidate, is certainly less secure than the other candidates.

While the cluster magnification increases the effective depth of the observations, the source-plane area that is surveyed at high redshift decreases inversely proportional to the magnification factor. The A1703 WFC3/IR image field of view is 4.6 arcmin$^2$, but we estimate that we are effectively surveying only ∼0.9 arcmin$^2$ in the $z \sim 7$ source plane. Thus, we derive a simple estimate of the number density of $z \sim 7$ sources in A1703 of 7.8 arcmin$^{-2}$. Typically, blank field surveys such as the HUDF09 and its two parallel fields (Bouwens et al. 2011a; Oesch et al. 2010b) find ∼3.5–4.3 $z \sim 7$ sources per arcmin$^2$. While our number density is larger than that found in typical blank fields, if we allow for the possibility that zD7 is a low-redshift interloper, we are left with six sources or 6.7 arcmin$^{-2}$. However, we note that cosmic variance in the number counts of high-redshift sources is significant in these relatively small-area *HST* fields (Trenti & Stiavelli 2008), especially the cluster fields with their significantly reduced area in the high-redshift source plane.

We can place the observations of A1703 in context with those obtained for a small, but growing, sample of strong lensing clusters with high-quality optical and NIR multiband data. While Hall et al. (2011) have reported the discovery of 10 $z_{850}$-dropouts behind the Bullet Cluster (Hall et al. 2011), most cluster lensing fields have produced at most 1–2 $z \gtrsim 7$ candidates. This includes NICMOS and WFC3/IR imaging of A1689 and the recent 16-band imaging of A383 and MACS1149 obtained by the CLASH MCT program. The apparent large variations in the number of $z \gtrsim 7$ candidates discovered behind lensing clusters suggests, not surprisingly, that $z \gtrsim 7$ galaxies may be highly clustered. One may therefore need to survey a large number of clusters to overcome the substantial large-scale structure effects.

## 8. SUMMARY

We report the discovery of a very bright, highly magnified LBG candidate (A1703-zD1) at $z \sim 6.7$ behind the massive galaxy cluster A1703. A1703-zD1 is 0.2 mag brighter than the recently discovered $z_{850}$-dropout candidate behind the Bullet Cluster (Hall et al. 2011) and 0.7 mag brighter than the current brightest known $z \sim 7.6$ galaxy A1689-zD1, identified behind the massive galaxy cluster A1689 (Bradley et al. 2008). We find a strong $z_{850} - J_{125}$ break of at least 1.7 mag and best-fit photometric redshift of $z = 6.7$. Using the Zitrin et al. (2010) cluster lensing model, we estimate a magnification of $\mu = 9$ at $z \sim 6.7$ at the position of A1703-zD1. The candidate is extended, spanning ∼4 kpc in the reconstructed source plane, and is resolved into three resolved star-forming knots. The source-plane deprojection shows that the star formation is occurring in compact knots of size ∼0.4 kpc.

Additionally, we find six other bright $z \sim 7$ $z_{850}$-dropout galaxy candidates behind A1703. One of these candidates, A1703-zD6, has been subsequently confirmed with Keck spectroscopy to be at $z = 7.045$ (Schenker et al. 2012). The candidates are observed with $H_{160}$-band magnitudes of 24.9–26.4, with a wide range of magnifications from 3 to 40. Their photometric redshifts are found to be in the range of $z_{\rm phot} = 6.4$–$8.8$, with a median redshift of 6.7. Using stellar population models to fit the rest-frame UV and optical fluxes for A1703-zD1 and A1703-zD4, we derive best-fit values for stellar masses $(0.7–3.0) \times 10^9\ M_\odot$, stellar ages 5–180 Myr, and star formation rates ∼7.8 $M_\odot$ yr$^{-1}$.

A1703-zD1, with a photometric redshift of $z \sim 6.7$ is the brightest observed $z \sim 7$ galaxy candidate found to date. We are planning to observe A1703-zD1 with near-IR spectroscopy to confirm its redshift and study its spectrum. Bright high-redshift galaxies such as these are valuable targets for ground-based spectroscopy and are pathfinding objects for future facilities such as the *James Webb Space Telescope*.

We thank Ivo Labbé and Valentino González for assistance with the *Spitzer*/IRAC photometry. We also thank the anonymous referee whose comments and suggestions significantly improved the quality and clarity of this work. ACS was developed under NASA contract NAS 5-32865, and this research has been supported by NASA grants NAG5-7697 and HST-GO10150.01-A and by an equipment grant from Sun Microsystems, Inc. The Space Telescope Science Institute is operated by AURA Inc., under NASA contract NAS5-26555. Archival data were obtained from observations made by the *Spitzer Space Telescope*, which is operated by the Jet Propulsion Laboratory, California Institute of Technology under NASA contract 1407.

## REFERENCES

Allen, S. W., Edge, A. C., Fabian, A. C., et al. 1992, MNRAS, 259, 67
Benítez, N. 2000, ApJ, 536, 571
Benítez, N., Ford, H., Bouwens, R., et al. 2004, ApJS, 150, 1
Bertin, E., & Arnouts, S. 1996, A&AS, 117, 393
Blakeslee, J. P., Anderson, K. R., Meurer, G. R., Benítez, N., & Magee, D. 2003, in ASP Conf. Ser. 295, Astronomical Data Analysis Software and Systems XII, ed. H. E. Payne, R. I. Jedrzejewski, & R. N. Hook (San Francisco, CA: ASP), 257
Bouwens, R. J., Illingworth, G. D., Bradley, L. D., et al. 2009, ApJ, 690, 1764
Bouwens, R. J., Illingworth, G. D., Labbe, I., et al. 2011a, Nature, 469, 504
Bouwens, R. J., Illingworth, G. D., Oesch, P. A., et al. 2011b, ApJ, 737, 90
Bouwens, R. J., Illingworth, G. D., Oesch, P. A., et al. 2010a, ApJ, 709, L133
Bouwens, R. J., Illingworth, G. D., Oesch, P. A., et al. 2010b, ApJ, 708, L69
Bradley, L. D., Bouwens, R. J., Ford, H. C., et al. 2008, ApJ, 678, 647
Bruzual, G., & Charlot, S. 2003, MNRAS, 344, 1000
Bunker, A. J., Wilkins, S., Ellis, R. S., et al. 2010, MNRAS, 409, 855
Calzetti, D., Armus, L., Bohlin, R. C., et al. 2000, ApJ, 533, 682
Chabrier, G. 2003, PASP, 115, 763
Coe, D., Benítez, N., Sánchez, S. F., et al. 2006, AJ, 132, 926
Dow-Hygelund, C. C., Holden, B. P., Bouwens, R. J., et al. 2005, ApJ, 630, L137
Egami, E., Kneib, J.-P., Rieke, G. H., et al. 2005, ApJ, 618, L5
Finkelstein, S. L., Papovich, C., Giavalisco, M., et al. 2010, ApJ, 719, 1250

Förster Schreiber, N. M., van Dokkum, P. G., Franx, M., et al. 2004, ApJ, 616, 40
Franx, M., Illingworth, G. D., Kelson, D. D., van Dokkum, P. G., & Tran, K. 1997, ApJ, 486, L75
Frye, B., Broadhurst, T., & Benítez, N. 2002, ApJ, 568, 558
Gonzalez, V., Labbe, I., Bouwens, R., et al. 2011, ApJ, 735, L34
Grogin, N. A., Kocevski, D. D., Faber, S. M., et al. 2011, ApJS, 197, 35
Hall, N., Bradac, M., Gonzalez, A. H., et al. 2011, (arXiv:1101.4677)
Iye, M., Ota, K., Kashikawa, N., et al. 2006, Nature, 443, 186
Knapp, G. R., Leggett, S. K., Fan, X., et al. 2004, AJ, 127, 3553
Kneib, J.-P., Ellis, R. S., Santos, M. R., & Richard, J. 2004, ApJ, 607, 697
Koekemoer, A. M., Faber, S. M., Ferguson, H. C., et al. 2011, ApJS, 197, 36
Kron, R. G. 1980, ApJS, 43, 305
Labbé, I., Bouwens, R., Illingworth, G. D., & Franx, M. 2006, ApJ, 649, L67
Labbé, I., González, V., Bouwens, R. J., et al. 2010a, ApJ, 716, L103
Labbé, I., González, V., Bouwens, R. J., et al. 2010b, ApJ, 708, L26
Limousin, M., Richard, J., Kneib, J., et al. 2008, A&A, 489, 23
Lorenzoni, S., Bunker, A., Wilkins, S., et al. 2011, MNRAS, 414, 1455
Madau, P. 1995, ApJ, 441, 18
Malhotra, S., & Rhoads, J. E. 2004, ApJ, 617, L5
McLure, R. J., Dunlop, J. S., Cirasuolo, M., et al. 2011, MNRAS, 418, 2074
McLure, R. J., Dunlop, J. S., de Ravel, L., et al. 2011, ArXiv e-prints
Miralda-Escude, J., & Rees, M. J. 1998, ApJ, 497, 21
Oesch, P. A., Bouwens, R. J., Carollo, C. M., et al. 2010a, ApJ, 709, L21
Oesch, P. A., Bouwens, R. J., Illingworth, G. D., et al. 2010b, ApJ, 709, L16
Oke, J. B. 1974, ApJS, 27, 21
Overzier, R. A., Heckman, T. M., Kauffmann, G., et al. 2008, ApJ, 677, 37
Postman, M., Coe, D., Benitez, N., et al. 2011, ApJ, in press (arXiv:1106.3328)
Richard, J., Pei, L., Limousin, M., Jullo, E., & Kneib, J. P. 2009, A&A, 498, 37
Salpeter, E. E. 1955, ApJ, 121, 161
Santos, M. R. 2004, MNRAS, 349, 1137
Schenker, M. A., Stark, D. P., Ellis, R. S., et al. 2012, ApJ, 744, 179
Stark, D. P., Ellis, R. S., Chiu, K., Ouchi, M., & Bunker, A. 2010, MNRAS, 408, 1628
Swinbank, A. M., Webb, T. M., Richard, J., et al. 2009, MNRAS, 400, 1121
Trenti, M., Bradley, L. D., Stiavelli, M., et al. 2011, ApJ, 727, L39
Trenti, M., & Stiavelli, M. 2008, ApJ, 676, 767
Yan, H., Yan, L., Zamojski, M. A., et al. 2011, ApJ, 728, L22
Zheng, W., Bradley, L. D., Bouwens, R. J., et al. 2009, ApJ, 697, 1907
Zitrin, A., Broadhurst, T., Coe, D., et al. 2011, MNRAS, 413, 1753
Zitrin, A., Broadhurst, T., Umetsu, K., et al. 2010, MNRAS, 408, 1916